RSC Advances

# A 3D Hierarchical Magnetic Fe@Pt/Ti(OH)4 Nanoarchitecture for Sinter-Resistant Catalyst



| | |
|---|---|
| Journal: | *RSC Advances* |
| Manuscript ID: | RA-ART-07-2015-013887 |
| Article Type: | Paper |
| Date Submitted by the Author: | 15-Jul-2015 |
| Complete List of Authors: | Zhang, Chao; Chemistry and Chemical Engineering of Southeast University,<br>Zhou, Yuming; Southeast University,<br>Zhang, yiwei; Southeast University, School of Chemistry and Chemical Engineering<br>Zhang, Zewu; Southeast University,<br>Wang, Qianli; School of Chemistry and Chemical Engineering, Southeast University,<br>Xu, Yuanmei; Southeast University, |
| | |

# A 3D Hierarchical Magnetic Fe@Pt/Ti(OH)$_4$ Nanoarchitecture for Sinter-Resistant Catalyst

Chao Zhang, Yuming Zhou* , Yiwei Zhang*, Zewu Zhang, Yuanmei Xu, Qianli Wang

School of Chemistry and Chemical Engineering, Southeast University, Jiangsu Optoelectronic Functional Materials and Engineering Laboratory, Nanjing 211189, China

## Abstract

Recently, the novel morphological nanocomposites have attracted an increasing attention due to the unique features. In this work, a 3D hierarchical magnetic Fe@Pt/Ti(OH)$_4$ nanoarchitecture has been synthesized successfully. TEM images were used to confirm the success of each of the synthesis steps, and the reduction of 4-NP to 4-AP was employed to evaluate the catalytic performance. The large surface area and nanorods structure guarantee a good catalytic performance. Besides, the as-prepared nanocapsule shows an excelent anti-sintering property for the physical barrier effects of Ti(OH)$_4$ nanorods. The sample calcined at 700 °C showed the highest catalytic activity in our work due to the decomposition of Ti(OH)$_4$. Finally, the synthesized Fe@Pt/Ti(OH)$_4$ nanocomposite could be easily recycled and shows a well recyclability.

---

Corresponding author: Yuming Zhou

E-mail: fchem@163.com;

Tel: +86 25 52090617;

Fax: +86 25 52090617.

**Key Words:** $Ti(OH)_4$, $\alpha$-$Fe_2O_3$, Pt nanocatalyst, Thermal stability

## 1. Introduction

Traditionally, Platinum catalysts play a key role in various chemical processes such as methanol oxidation, polymer electrolyte membrane fuel cells, CO oxidation, and petroleum cracking.[1-4] However, in practical applications of high temperature (typically higher than 300 °C), Pt NPs tend to lose their specific surface area due to the aggregation of metal NPs and thus catalytic activity.[3] So it is meaningful to find a way to improve the thermal stability of noble metal catalysts. Recent studies have shown that metallic nanoparticles can be greatly stabilized against coalescence using the method of encapsulation within various inorganic layers.[5-10] Besides, various methods have been developed to construct channels for reactant molecules to reach buried active points.[3, 5, 11, 12] But, in fact, supported catalysts generally performe better than surface encapsulated metal catalyst due to the shorter diffusion path.[13-15] Moreover the supported catalysts with inlaid metal NPs shown better sinter-resistant ability than traditional supported catalsts.[9, 12, 16]

Different kinds of 3D hierarchical nanoarchitectures have been prepared readily due to the recent advances in colloid chemistry.[17-21] And the 3D nanostructures are suitable to be used as support meatrials for the high surface area. Furthermore the catalytic performances are remarkably affected by the interactions between metal and support materials. The titanium compound support (expecially $TiO_2$) has been studyed by countless researchers.[6, 22-24] However, few people studied the performance of

$Ti(OH)_4$ when serve as support materials specially, especially, at different temperature. $Ti(OH)_4$ nanocomposite could be synthesized by the corrosive attack of hydroxyl groups to $TiO_2$.[25, 26] Consequently, it is meaningful to synthesize a nanoarchitecture with a 3D hierarchical $Ti(OH)_4$ support. In addition, ellipsoidal $\alpha$-$Fe_2O_3$ could be reduced to magnetic Fe with $H_2$ and the synthesized nanocapsule would show a higher diffusion for the high aspect ratio.[22, 27-29] So it is reasonable to chose the ellipsoidal $\alpha$-$Fe_2O_3$ as template.

Herein, we report a 3D hierarchical ant-sintering catalytic system consisting of $Ti(OH)_4$ nanorods with inlaid Pt NPs and a ellipsoidal Fe core (Fig. 3b). In this system, the 3D hierarchical $Ti(OH)_4$ nanorods (Fig. 3a) could act as a physical barrier to prevent the sintering of metal NPs and guarantee the catalyst of a high surface area. More importantly, part of the inner Pt NPs exposed to outside after the treatment of NaOH solution (Fig. 8c) and contacted with chemical species directly without barrier layer resulting to a short diffusion path. Consequently, the new catalyst may show not only a good catalytic property but also an increased stability against sintering. The fabrication of Fe@Pt/$Ti(OH)_4$ catalytic system is depicted in Fig. 1. Firstly, $\alpha$-$Fe_2O_3$ NPs were prepared via a hydrothermal method, and then, coated with a layer of carbon, Pt NPs, $TiO_2$ and mesoporous $SiO_2$ ($mSiO_2$) successively. The synthesized $\alpha$-$Fe_2O_3$@C/Pt/$TiO_2$/$mSiO_2$ nanocapsules were calcined at 500 °C for 3 h to remove carbon layers. Then the calcined nanocomposites were treated with concentrated NaOH solution at room temperature to remove the $mSiO_2$ layer and ,meanwhile, transform the $TiO_2$ layer into $Ti(OH)_4$ nanorods. Lastly, the obtained

$\alpha$-$Fe_2O_3$@Pt/$Ti(OH)_4$ nanocapsules were treated with $H_2$ to reduce the $\alpha$-$Fe_2O_3$ core to magnetic Fe. The synthesized catalyst was evaluated through the reduction of 4-nitrophenol (4-NP) to 4-aminophenol (4-AP). It was found that the obtained $\alpha$-$Fe_2O_3$@Pt/$Ti(OH)_4$ samples exhibited a well anti-sintering property and recyclability.

## 2. Experiment

### 2.1. Materials

potassium tetrachoroplatinate ($K_2PtCl_4$, ≥96%), 3-aminopropyl-triethoxysilane (APTES), sodium borohydride ($NaBH_4$), Glucose, cetyltrimethylammonium bromide (CTAB), trisodium citrate, and 4-nitrophenol (≥99%) were purchased from Aldrich. $FeCl_3$, $KH_2PO_4$, tetraethyl orthosilicate (TEOS), tetrabutyl titanate (98%), isopropanol, ethanol, and ammonia solution (25–28%) were analytical grade, and all of them were purchased from Sinopharm Chemical Reagent Co., Ltd. Deionized (DI) water was used in all experiment. All chemicals were used as received without furtherb purification.

### 2.2. Synthesis

Synthesis of ellipsoidal $\alpha$-$Fe_2O_3$ NPs: Monodispersed spindle shaped $\alpha$-$Fe_2O_3$ nanotemplate were fabricated according to the method described by Chen and co-workers.[30] Typically, An aqueous solution (100 mL) of $FeCl_3$ ($2.0 \times 10^{-2}$ M) and $KH_2PO_4$ ($4.0 \times 10^{-4}$ M) were aged at 105 °C for 45 h. The resulting precipitate was centrifuged and washed three times with water respectively. The collected products

were dried at 60 °C for 6 h.

Carbon layer coating : 8 g of glucose and 80 mL doubly deionized water were added to a 100 mL Teflon-lined stainless steel autoclave, the mixture was stirred vigorously for a while. Then 0.1 g of the as-prepared α-$Fe_2O_3$ was added to the above transparent solution. The autoclave was sealed and heated at 160 °C in an oven for 12 h to attain the desired shell thickness. The obtained samples were centrifuged to remove supernatant liquid.

Pt NPs loading: The as-obtained α-$Fe_2O_3$@C NPs were added to a solution of isopropanol (100 mL) and APTES (0.5 mL), and heated up to 80 °C for 12 h. The result mixture was collected by centrifugation and washed with isopropanol three times. Then the as-functionalized α-$Fe_2O_3$@C NPs were dispersed into a mixture of DI water (100 mL), $K_2PtCl_4$ (2 mL, 7.11 mg/mL), and trisodium citrate (5 mL, 20 mg/mL) at room temperature (RT). After magnetic stirring for 30 min, fresh sodium borohydride (10 mL, 0.008 mg/mL) was immediately injected to the solution under vigorous stirring. After stirring at RT for 12 h, α-$Fe_2O_3$@C/Pt composition was isolated by centrifugation and the collected products were dried at 60 °C for 6 h.

$TiO_2$ coating: The $TiO_2$ layer was prepared using a method developed by Yin *et al.*[24] The α-$Fe_2O_3$@C/Pt particles were dispersed in a mixture of hydroxypropyl cellulose (HPC, 0.2 g), ethanol (70 mL), and de-ionized water (0.2 mL). After stirring for 30 min, titanium tert-butoxide (TBOT, 2 mL) in 20 mL ethanol was injected into the mixture slowly. After injection, the temperature was increased to 85 °C at 900 rpm stirring under refluxing conditions for 100 min. The precipitate was isolated using

centrifugation, washed with ethanol, and re-dispersed in 5 mL of ethanol to give α-$Fe_2O_3$@C/Pt/$TiO_2$ nanocomposites. In order to increase the thickness of the $TiO_2$ layer, the above coating procedure was repeated multiple times.

$mSiO_2$ coating: The $mSiO_2$ layer was constructed via a modified Stöber method using cetyltrimethylammonium bromide (CTAB) as template.[31] The as-obtained α-$Fe_2O_3$@C/Pt/$TiO_2$ NPs were added into a solution containing de-ionized water (60 mL), ethanol(30 mL), CTAB (150 mg), and ammonia solution (0.55 mL) under mildly stirring. Then tetraethyl orthosilicate (TEOS, 0.2 mL) was slowly injected into the solution and stirring for 6 h. The α-$Fe_2O_3$@C/Pt/$TiO_2$/$mSiO_2$ nanoparticles were obtained by centrifugation and washed with ethanol several times.

Calcination and $SiO_2$ etching: α-$Fe_2O_3$@C/Pt/$TiO_2$/$mSiO_2$ sample was calcined in air at 500 °C for 3 h to remove organic compounds mostly and crystallize the amorphous $TiO_2$. Then the calcined samples were dispersed in 50 mL water under sonication. Then an aqueous NaOH solution (0.5 M) was added to the above solution at room temperature. After etching for 24 h, the α-$Fe_2O_3$@Pt/$Ti(OH)_4$ NPs were finally isolated by centrifugation and washed 5 times with de-ionized water.

$H_2$ reduction: the powder was transferred to a tube furnace with ultrapure hydrogen (99.99%) flow at 500 °C for 4 h. The product was then naturally cooled to room temperature and the 3D hierarchical magnetical Fe@Pt/$Ti(OH)_4$ nanocatalysts were synthesized finally.

**2.3. Characterization**

Transmission electron microscopy (TEM) experiments were conducted on a

JEM-1230 microscope operated at 100 kV. The TEM samples were prepared by transferring one drop of sample dispersion in ethanol onto a carbon-coated copper grid and then dried in air. X-ray diffraction (XRD) patterns were recorded on a Bruker D8 Advance Diffractometer (Germany) with Cu Kα radiation (λ = 1.5406 Å). Thermo Gravimetric Analysis (TGA) of the samples was performed with Rigaku ThermoPlus TG8120 system from room temperature to 800 °C at the rate of 10 °C /min under air. UV-Vis spectra analysis was performed on a Shimadzu UV 3600 spectrometer. Scanning electron microscope (SEM) was performed on a Hitachi S-3400N scanning electron microscope and energy dispersion X-ray analysis (EDX) were conducted on a JEM-1230 microscope operated at 100 kV. The nitrogen adsorption and desorption isotherms were measured at −196 °C on an ASAP 2020 (Micromertics USA). The specific surface area was determined from the linear part of the BET equation ($P/P_0$ =0.05–0.25). The pore size distribution was derived from the desorption branch of the $N_2$ isotherm using the Barrett–Joyner–Halenda (BJH) method.

**2.4. Catalytic evaluation**

The reduction of 4-NP to 4-AP was chosen as a model reaction to study the catalytic properties. In a typical run, 4-NP (0.03 mL, 0.01 M, aqueous solution), $H_2O$ (2 mL) and nanocatalyst (0.5 mL ,1 mg/mL) were mixed with freshly prepared $NaBH_4$ (0.5 mL, 0.25 M, aqueous solution) in a quartz cell (3.0 mL). The absorption spectra were recorded on a UV-Vis spectrophotometer at a regular interval in the range of 250-700 nm. For the recycling experiment, the catalysts were collected by magnet, washed

with deionized water, dried at 60 °C and reused in the next cycle.

## 3. Results and discussion

### 3.1. Characterization of Fe@Pt/Ti(OH)$_4$ nanocapsules

The main experimental procedures and the observations are summarized in Fig. 2 and 3. Just as can be seen from Fig. 2a, the synthesized α-$Fe_2O_3$ NPs have an elliptical morphology and a high aspect ratio. And the α-$Fe_2O_3$ particles have been coated with a layer of carbon (*ca.* 19 nm in thickness, Fig. 2c) with glucose as carbon source. In this process, various chemical reactions took place under hydrothermal conditions and resulted in a complex mixture of organic compounds.[32] The surfaces of α-$Fe_2O_3$/C particle are further derivatized with a monolayer of the coupling agent 3-aminopropyltriethoxysilane (APTES) by heating the mixture in isopropanol at 80 °C to functionalize the surfaces with amino groups.[33] Then citrate-stabilized Pt nanoparticles are able to adsorb on the surface of carbon layer as the result of the strong chemical affinity between Pt and primary amines.[5, 24] Furthermore, α-$Fe_2O_3$@C/Pt composite were coated with a layer of amorphous $TiO_2$, by using titanium tetrabutoxide (TBOT) as $TiO_2$ precursor, hydroxypropyl cellulose (HPC) as a surfactant, and ethanol as the reaction medium.[6, 34] Pt NPs between the layers of carbon and $TiO_2$ can been seen obviously (Fig. 4d), indicating the successful synthesis of α-$Fe_2O_3$@C/Pt/$TiO_2$ nanocomposite. After that, a layer of mesoporous $SiO_2$ ($mSiO_2$) were constructed with CTAB as pore-generating agents (Fig. 2d).[11] The synthesized α-$Fe_2O_3$@C/Pt/$TiO_2$/$mSiO_2$ nanocapsules were calcined at 500 °C for 3 h

to remove carbon layers. Just as shown in Fig. S1b, a gap between α-$Fe_2O_3$ and the Pt/$TiO_2$/m$SiO_2$ shell appears after calcination. It is well known that the crystallinity of $TiO_2$ can be improved by calcination.[34] Meanwhile, importantly, the burned carbon layer can provide enough space for the growth of $TiO_2$ into crystal grains. Besides the outer m$SiO_2$ layer could prevent the collapse of the $TiO_2$ layer.[12, 35] Just as shown in Fig. 4c, the sample of α-$Fe_2O_3$@C/Pt/$TiO_2$ without m$SiO_2$ layer protection collapsed after calcination at 500 °C, thus it is necessary to coat a layer of m$SiO_2$ layer outside.

Then, the m$SiO_2$ layer could be removed with concentrated NaOH solution at room temperature and, importantly, the 3D hierarchical nanoarchitecture can be synthesized successfully in one step (Fig. 4a and b). The $TiO_2$ nanocrystals could react with concentrated NaOH solution in wet-chemical processes, yielding $Ti(OH)_4$ material.[25, 26] From the XRD pattern of Fig. 5, the peaks at 2θ= 25.4°, 37.9°, 47.7°, 55.1° and 62.5° match with the thermal treated $Ti(OH)_4$ at 500 °C.[36] Besides, the as synthesized nanorods disappeared after the treatment of dilute HCl solution (10 Wt%) at room temperature and, accordingly, the surface of spindle α-$Fe_2O_3$ particles became uneven due to the erosion of HCl solution (Fig. S2b). In addition, it is well known that $Ti(OH)_4$ will break up into $TiO_2$ and $H_2O$ when calcined at high temperature.[37-39] Just as shown in Fig. 6b and 3d, the weight lost obviously when the temperature above 500 °C and the nanorods disappeared replaced by numerous tiny crystals after calcination at 700 °C. Besides, the elliptical morphology remained without collapse. The selected area electron diffraction (SAED) and XRD patterns of calcined α-$Fe_2O_3$@Pt/$Ti(OH)_4$ sample at 500 °C indicate the existance of Pt (Fig. 5 and S2a )

and the energy-dispersive X-ray mapping analysis confirms the well dispersion of Pt, Ti and Fe elements (Fig. 7a).

As shown in Fig. 4a, the synthesized $Ti(OH)_4$ nanorods are intricately distributed on the surface of $\alpha$-$Fe_2O_3$, and the SEM image of Fig. 4b is consistent to the hierarchical nanostructures. From the XRD pattern of Fig. S3, the peaks of $\alpha$-$Fe_2O_3$ were replaced by the peaks of Fe indicating the reduction of $Fe_2O_3$ to Fe after $H_2$ reduction treatment. What's more, the peaks of Pt and $Ti(OH)_4$ cannot be observed may due to the high dispersion of Pt NPs and the strong diffractions of Fe compound.[22, 27] Besides, the week peak at $2\theta = 40.9^o$ may be attributed to the reflection from (113) plane of the rare residual $\alpha$-$Fe_2O_3$.[22] Interestingly, a core appears after $H_2$ reduction resulting a yolk-shell nanostructure and the hierarchical nanostructures maintained without destruction (Fig. 3b and c).

Then the effect of $TiO_2$ layer on thermal stability of the catalysts was tested. In generally, Pt NPs was inlaid in $TiO_2$ layer before calcination and the $TiO_2$ layer offers an physical barrier to prevent the sintering of individual Pt NPs.[12, 16] From Fig. 6a, the carbon layer could be removed mostly at 500 °C releasing a tremendous amount of heat. Therefore, in this work, $\alpha$-$Fe_2O_3$@C/Pt/$TiO_2$/$SiO_2$ should be calcined at 500 °C and the size of Pt NPs changed from 2.19 to 3.93 nm（Fig. 4d and 8a）. In contrast, the traditional "naked" (*i.e.*, without any physical barrier) $\alpha$-$Fe_2O_3$@$TiO_2$/Pt sample (TN) showed lower anti-sintering properties with a larger Pt size (*ca.* 4.43 nm in diameter, Fig. 8b). In order to contrast more clearly, the calcination temperature (CT) was increased to 700 °C and the differences in size between the two samples are

more striking, the Pt diameter of TN (*ca.* 13.45 nm in diameter) increased more quickly than α-$Fe_2O_3$@C/Pt/$TiO_2$/m$SiO_2$ sample (*ca.* 7.47 nm in diameter, Fig. 8c and d). Consequently the $TiO_2$ layer is quite effective in preserving the size of Pt NPs. Furthermore it should be noted that Pt NPs was encapsuled in the $TiO_2$ layer at first, so part of the Pt NPs may be still enbedded in $Ti(OH)_4$ nanorods after the treatment of alkali liquor, resulting a better thermal stability of the 3D hierarchical nanoarchitecture. And the excelent physical barrier effects of $TiO_2$ layer ensured a smaller diameter of Pt NPs before $H_2$ reduction process. Fig. 8c displays the TEM image of α-$Fe_2O_3$@Pt/$Ti(OH)_4$, some of the Pt NPs dispersed in the outer region of the spindle NPs rather than interior area. The open active sites contact with chemical species directly without barrier layer, which can result in a short diffusion path.

$N_2$ physisorption measurements were used to investigate the structure properties of α-$Fe_2O_3$@Pt/$Ti(OH)_4$ and traditional "naked" α-$Fe_2O_3$@$TiO_2$/Pt samples. Just as shown in Fig. 9, the samples exhibited a type IV curve according to the IUPAC nomenclature. The hysteresis loop of Fig. 9b at a high relative pressure (0.8–1.0) corresponds to the filling of the macropores produced by the stacking of α-$Fe_2O_3$@$TiO_2$/Pt NPs. More importantly, the sample of α-$Fe_2O_3$@Pt/$Ti(OH)_4$ has a larger specific surface area (115.1 $m^2g^{-1}$, Fig. 9a) than TN (15.4 $m^2g^{-1}$, Fig. 9b) due to the specially 3D hierarchical nanoarchitecture, leading to an improved catalytic performanced definitely.

### 3.2. Catalytic reduction of 4-nitrophenol

The activity of these catalysts were evaluated by the reduction of 4-NP to 4-AP with $NaBH_4$. It's ease to understand that, in this reaction, the value of apparent rate constant ($k_{app}$) decreaseed with the aggreation of Pt NPs. Thus, the reaction rate of 4-NP with $NaBH_4$ is related to the size of Pt NPs. From the above, we only need a simple reaction to get the value of $k_{app.}$ The reduction of 4-NP to 4-AP has been widely used as the model reaction of noble metal nanocatalyst for the low cost and ease of operation.[5, 40, 41] Thus, the thermal stability of the catalyst can be evaluated through the value of $k_{app}$.[12, 16, 27, 42] The reaction is fast in the presence of metallic surfaces and did not occur without noble metal catalysts, even in a long time.[31, 41, 43] Besides, the process could be regarded as a first-order reaction with excess amount of $NaBH_4$. Fig. 10a shows a typical UV-vis absorption change of the reaction by the addition of HN500, the absorption at 400 nm decreased and absorption at 295 nm increased, indicating the reduction of 4-NP and formation of 4-aminophenol (4-AP), respectively. And the isobestic point at 313 nm indicates the reaction proceeded precisely without any byproducts.[22] In all catalytic runs, the dosage of every reagent kept constant. Fig. 10b shows the linear relationships between $\ln(C_o/C_t)$ and reaction time ($C_t$ is the ordinate values of the absorption peak at 400 nm). According to the linear relationship, the apparent rate constant ($k_{app}$) could be obtained from the slopes of the straight lines. From Fig. 10b, the $k_{app}$ of HMN and HMN500 were 0.17243 and 0.14556 $min^{-1}$ respectively. The catalytic activity of HMN decreased slightly after the calcination at 500 °C for the increasing Pt NPs diameter from 4.15 to 4.48 nm (Fig. 11a and b). The little loss of reactivity indicates the excelent anti-sintering property of

the 3D hierarchical Fe@Pt/$Ti(OH)_4$ nanoarchitecture. However, interestingly, when CT changed from 500 °C to 700 °C, the rate constant didn't decrease but increasing significantly (0.2713 $min^{-1}$, Fig. 10b). The funny phenomenon can be ascribed to the decomposition of $Ti(OH)_4$ into $TiO_2$ and $H_2O$. Just as shown in Fig. 3d, the rod like structure was transformed into unnumbered nanocrystals due to the calcination treatment at 700 °C. Accordingly the nanorods structures disappeared. Besides, from Fig. S5, the (103) and (101) planes of $TiO_2$ could demonstrate the existance of $TiO_2$ after cancination. The higher interaction between Pt NPs and $TiO_2$ can promote the performance of the nanocatalyst.[12, 35] Moreover, a comparison of Fe@Pt/$Ti(OH)_4$ with other Pt-based nanocatalysts reported in other literature is required. From Table S1, it can be found that the Fe@Pt/$Ti(OH)_4$ catalyst in our experiment is much higher than the most reports for the catalytic reduction of 4-NP by $NaBH_4$.

Lastly, the recyclability of HMN nanocatalyst has been studied. As shown in Fig. 12, the samble can be separated easily within a few seconds because of the magnetic Fe core. Besides, the nanocatalyst could be reused for at least five times with a stable conversion of 95%, and the stable conversion indicated that most of the nanocatalyst could be separated using magnet. Besides the structure of the 3D hierarchical nanoarchitecture retained after five repeating catalytic cycles (Fig. 12c). By comparison, as for the TN500 sample, the conversion of 4-NP reduced rapidly after three cycles of catalytic tests.(Fig. S4a). The low reusability may be due to the massive loss of Pt NPs from surface.(Fig. S4b) The above results demonstrated that the microsized Fe@Pt/$Ti(OH)_4$ nanohybrids have a well recyclability also.

## 4. Conclusion

A 3D hierarchical magnetic Fe@Pt/$Ti(OH)_4$ nanoarchitecture catalyst has been prepared and characterized. The $Ti(OH)_4$ nanorods provide a physical barrier to slow down the migration of Pt NPs and thus effectively improve the anti-sintering. The nanoparticles maintained their paramecium-shaped core-shell configurations up to 500 °C. However, interestingly, the catalytic performance increased significantly after calcination at 700 °C in air due to the decomposition of $Ti(OH)_4$. Besides, the sample of Fe@Pt/$Ti(OH)_4$ shows an excellent reusability without obviously decrease of the catalytic activities even after five cycles. Future work will involve the synthesize of an novel morphology nanocomposite.

## Acknowledgments

The authors are grateful to the financial supports of National Natural Science Foundation of China (Grant No. 21376051, 21106017, 21306023 and 51077013), Natural Science Foundation of Jiangsu (Grant No.BK20131288), Fund Project for Transformation of Scientific and Technological Achievements of Jiangsu Province of China (Grant No. BA2011086), Specialized Research Fund for the Doctoral Program of Higher Education of China (Grant No.20100092120047), Key Program for the Scientific Research Guiding Found of Basic Scientific Research Operation Expenditure of Southeast University (Grant No. 3207043101) and Instrumental Analysis Fund of Southeast University.

**References**


1. Z. Cui, C. X. Guo and C. M. Li, *J. Mater. Chem. A*, 2013, **1**, 6687-6692.
2. S. Zhang, Y. Shao, G. Yin and Y. Lin, *J. Mater. Chem. A*, 2013, **1**, 4631-4641.
3. S. H. Joo, J. Y. Park, C. K. Tsung, Y. Yamada, P. D. Yang and G. A. Somorjai, *Nat. Mater.*, 2009, **8**, 126-131.
4. Y. Dai, B. Lim, Y. Yang, C. M. Cobley, W. Li, E. C. Cho, B. Grayson, P. T. Fanson, C. T. Campbell, Y. Sun and Y. Xia, *Angew. Chem. Int. Edit.*, 2012, **51**, 10692-10692.
5. J. P. Ge, Q. Zhang, T. R. Zhang and Y. D. Yin, *Angew. Chem. Int. Edit.*, 2008, **47**, 8924-8928.
6. J. B. Joo, M. Dahl, N. Li, F. Zaera and Y. Yin, *Energ. Environ. Sci.*, 2013, **6**, 2082-2092.
7. I. Lee, J. B. Joo, Y. Yin and F. Zaera, *Angew. Chem. Int. Ed. Engl.*, 2011, **50**, 10208-10211.
8. Q. Zhang, I. Lee, J. Ge, F. Zaera and Y. Yin, *Adv. Funct. Mater.*, 2010, **20**, 2201-2214.
9. P. Lu, C. T. Campbell and Y. Xia, *Nano Lett.*, 2013, **13**, 4957-4962.
10. J. Lee, J. C. Park and H. Song, *Adv. Mater.*, 2008, **20**, 1523-1528.
11. Y. Deng, D. Qi, C. Deng, X. Zhang and D. Zhao, *J. Am. Chem. Soc.*, 2008, **130**, 28-29.
12. Z. Zhang, Y. Zhou, Y. Zhang, S. Xiang, S. Zhou and X. Sheng, *RSC Adv.*, 2014, **4**, 7313-7320.

13. P. Zhang, R. Li, Y. M. Huang and Q. W. Chen, *ACS Appl. Mater. Inter.*, 2014, **6**, 2671-2678.

14. M. Cargnello, N. L. Wieder, T. Montini, R. J. Gorte and P. Fornasiero, *J. Am. Chem. Soc.*, 2010, **132**, 1402-1409.

15. K. Bakhmutsky, N. L. Wieder, M. Cargnello, B. Galloway, P. Fornasiero and R. J. Gorte, *Chemsuschem*, 2012, **5**, 140-148.

16. S. Xiang, Y. Zhou, Y. zhang, Z. Zhang, X. Sheng, S. Zhou and Z. Yang, *Dalton Trans.*, 2014, **43**, 11039-11047.

17. W. Tang, W. Li, X. Shan, X. Wu and Y. Chen, *Mater. Lett.*, 2015, **140**, 95-98.

18. W.-J. Ong, L.-L. Tan, S.-P. Chai, S.-T. Yong and A. R. Mohamed, *Nanoscale*, 2014, **6**, 1946-2008.

19. Z. Haider and Y. S. Kang, *ACS Appl. Mater. Inter.*, 2014, **6**, 10342-10352.

20. T. J. Athauda, J. G. Neff, L. Sutherlin, U. Butt and R. R. Ozer, *ACS Appl. Mater. Inter.*, 2012, **4**, 6917-6926.

21. Z. Sun, J. H. Kim, Y. Zhao, F. Bijarbooneh, V. Malgras, Y. Lee, Y.-M. Kang and S. X. Dou, *J. Am. Chem. Soc.*, 2011, **133**, 19314-19317.

22. C. Zhang, Y. Zhou, Y. Zhang, Q. Wang and Y. Xu, *RSC Adv.*, 2015, **5**, 12472-12479.

23. Y. Lu, B. C. Jiang, D. L. Cao, Z. J. Zhang, X. Zhang, R. R. Ji and Y. J. Gao, *Pain*, 2014, **155**, 2618-2629.

24. Q. Zhang, D. Q. Lima, I. Lee, F. Zaera, M. Chi and Y. Yin, *Angew. Chem. Int. Ed.*, 2011, **50**, 7088-7092.

25. C. M. d. Assis, L. C. d. O. Vercik, M. L. d. Santos, M. V. L. Fook and A. C. Guastaldi, *Mat. Res.*, 2005, **8**, 207-211.

26. F. J. Gil, A. Padrós, J. M. Manero, C. Aparicio, M. Nilsson and J. A. Planell, *Mat. Sci. Eng. C-Mter.*, 2002, **22**, 53-60.

27. Z. Zhang, Y. Zhou, Y. Zhang, S. Zhou, S. Xiang, X. Sheng and P. Jiang, *J. Mater. Chem. A*, 2015, **3**, 4642-4651.

28. C. Hu, X. Zhai, Y. Zhao, K. Bian, J. Zhang, L. Qu, H. Zhang and H. Luo, *Nanoscale*, 2014, **6**, 2768-2775.

29. G. Yun, Z. Hassan, J. Lee, J. Kim, N.-S. Lee, N. H. Kim, K. Baek, I. Hwang, C. G. Park and K. Kim, *Angew. Chem. Int. Ed.*, 2014, **53**, 6414-6418.

30. H. Chen, D. Sulejmanovic, T. Moore, D. C. Colvin, B. Qi, O. T. Mefford, J. C. Gore, F. Alexis, S. J. Hwu and J. N. Anker, *Chem. Mater.*, 2014, **26**, 2105-2112.

31. Y. Deng, Y. Cai, Z. Sun, J. Liu, C. Liu, J. Wei, W. Li, Y. Wang and D. Zhao, *J. Am. Chem. Soc.*, 2010, **132**, 8466-8473.

32. Y. Wan, Y. L. Min and S. H. Yu, *Langmuir*, 2008, **24**, 5024-5028.

33. I. Lee, Q. Zhang, J. Ge, Y. Yin and F. Zaera, *Nano Res.*, 2010, **4**, 115-123.

34. J. B. Joo, Q. Zhang, I. Lee, M. Dahl, F. Zaera and Y. Yin, *Adv. Funct. Mater.*, 2012, **22**, 166-174.

35. Z. Zhang, Y. Zhou, Y. Zhang, S. Zhou, J. Shi, J. Kong and S. Zhang, *Dalton Trans.*, 2013, **42**, 5004-5012.

36. V. Legrand, O. Merdrignac-Conanec, W. Paulus and T. Hansen, *J. Phys. Chem. A*, 2012, **116**, 9561-9567.

37. H. S. P. Fard and H. Baharvandi, *B. Mater. Sci.*, 2011, **34**, 883-886.

38. W. J. Kim, B. Veriansyah, J. D. Kim and S. G. Oh, *J. Ceram. Process Res.*, 2008, **9**, 88-92.

39.T. Kokubo, *Acta. Mater.*, 1998, **46**, 2519-2527.

40. J. Lee, J. C. Park and H. Song, *Adv. Mater.*, 2008, **20**, 1523-1528.

41. J. C. Park and H. Song, *Nano Research*, 2010, **4**, 33-49.

42. Z. Zhang, Y. Zhou, Y. Zhang, X. Sheng, S. Zhou and S. Xiang, *Rsc Adv.*, 2014, **4**, 40078-40084.

43. X. Fang, X. Zhao, W. Fang, C. Chen and N. Zheng, *Nanoscale*, 2013, **5**, 2205-2218.

Fig. 1 Synthetic procedure of Fe@Pt/$Ti(OH)_4$ nanocapsule.

Fig. 2 TEM images of (a) α-$Fe_2O_3$, (c) α-$Fe_2O_3$@C, (d) α-$Fe_2O_3$@C/Pt/$TiO_2$/$mSiO_2$. SAED pattern obtained from (b) α-$Fe_2O_3$ NPs.

Fig. 3 TEM images of (a) $Ti(OH)_4$ nanorods, (b) Fe@Pt/$Ti(OH)_4$, (d) calcined Fe@Pt/$Ti(OH)_4$ at 700 °C. And SEM image of (c) Fe@Pt/$Ti(OH)_4$.

Fig. 4 TEM images of (a) α-$Fe_2O_3$@Pt/$Ti(OH)_4$, (c) calcined α-$Fe_2O_3$@C/Pt/$TiO_2$ at 500 °C without $mSiO_2$ protection, (d) the magnified α-$Fe_2O_3$@C/Pt/$TiO_2$. And SEM image of (b) α-$Fe_2O_3$@Pt/$Ti(OH)_4$.

Fig. 5 XRD pattern of cancined α-$Fe_2O_3$@Pt/$Ti(OH)_4$ at 500 °C.

Fig. 6 TGA curves for (a) α-$Fe_2O_3$@C/Pt/$TiO_2$/$mSiO_2$ and (b) α-$Fe_2O_3$@Pt/$Ti(OH)_4$.

Fig. 7 (a) EDX mapping analysis and (b) EDX analysis of Fe@Pt/$Ti(OH)_4$.

Fig. 8 TEM images of (a) calcined α-$Fe_2O_3$@C/Pt/$TiO_2$/$mSiO_2$ at 500 °C, (b) calcined TN at 500 °C (TN500), (c) calcined α-$Fe_2O_3$@C/Pt/$TiO_2$/$mSiO_2$ at 700 °C and then treated with concentrated NaOH solution, (d) calcined TN at 700 °C (TN700). All the samples were calcined in air for 4 h.

Fig. 9 Nitrogen adsorption–desorption isotherms of (a) α-$Fe_2O_3$@Pt/$Ti(OH)_4$ and (b) traditional "naked" α-$Fe_2O_3$@$TiO_2$/Pt sample. The inset is the pore size distribution.

Fig. 10 (a) Variation in UV-vis spectra at 3 min intervals for the 4-NP reduction in the presence of Fe@Pt/Ti(OH)$_4$. (b) ln($C_t/C_0$) versus the reaction time over different samples: (1) Fe@Pt/Ti(OH)$_4$ (HMN), (2) calcined HMN at 500 ℃ in air (HMN500), (3) calcined HMN at 700°C in air (HMN700).

Fig. 11 TEM images of (a) Fe@Pt/Ti(OH)$_4$ (HMN), (b) calcined HMN at 500 ℃ in air for 4h (HMN500)

Fig. 12 (a) $C_t/C_0$ as a function of the reaction time in five successive reduction using HMN catalyst, (b) the images of magnetic separation, (c) TEM image of the final HMN catalyst.

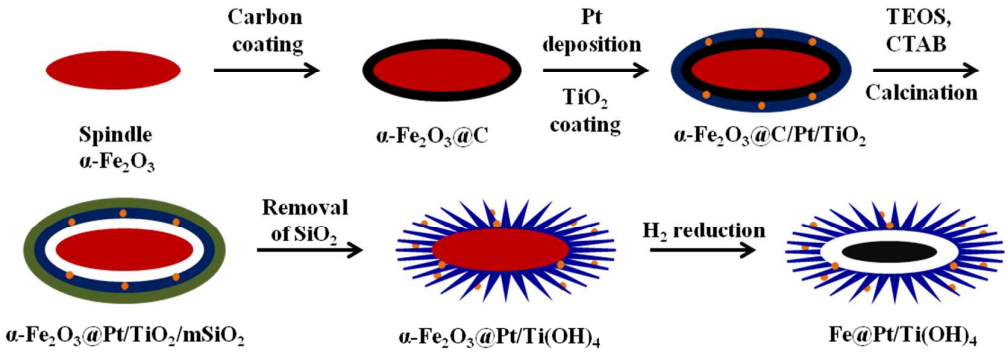


Fig. 1 Synthetic procedure of Fe@Pt/Ti(OH)$_4$ nanocapsule.

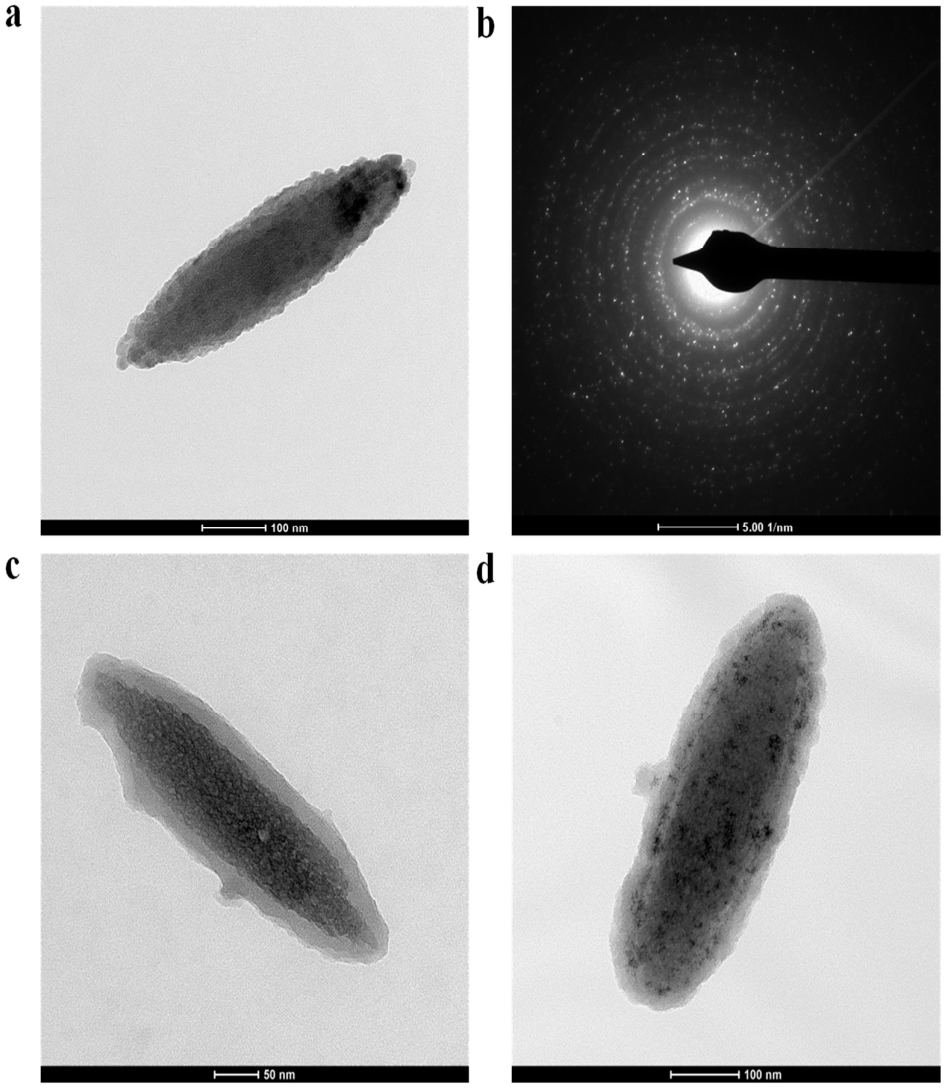


Fig. 2 TEM images of (a) α-$Fe_2O_3$, (c) α-$Fe_2O_3$@C, (d) α-$Fe_2O_3$@C/Pt/$TiO_2$/m$SiO_2$.

SAED pattern obtained from (b) α-$Fe_2O_3$ NPs.

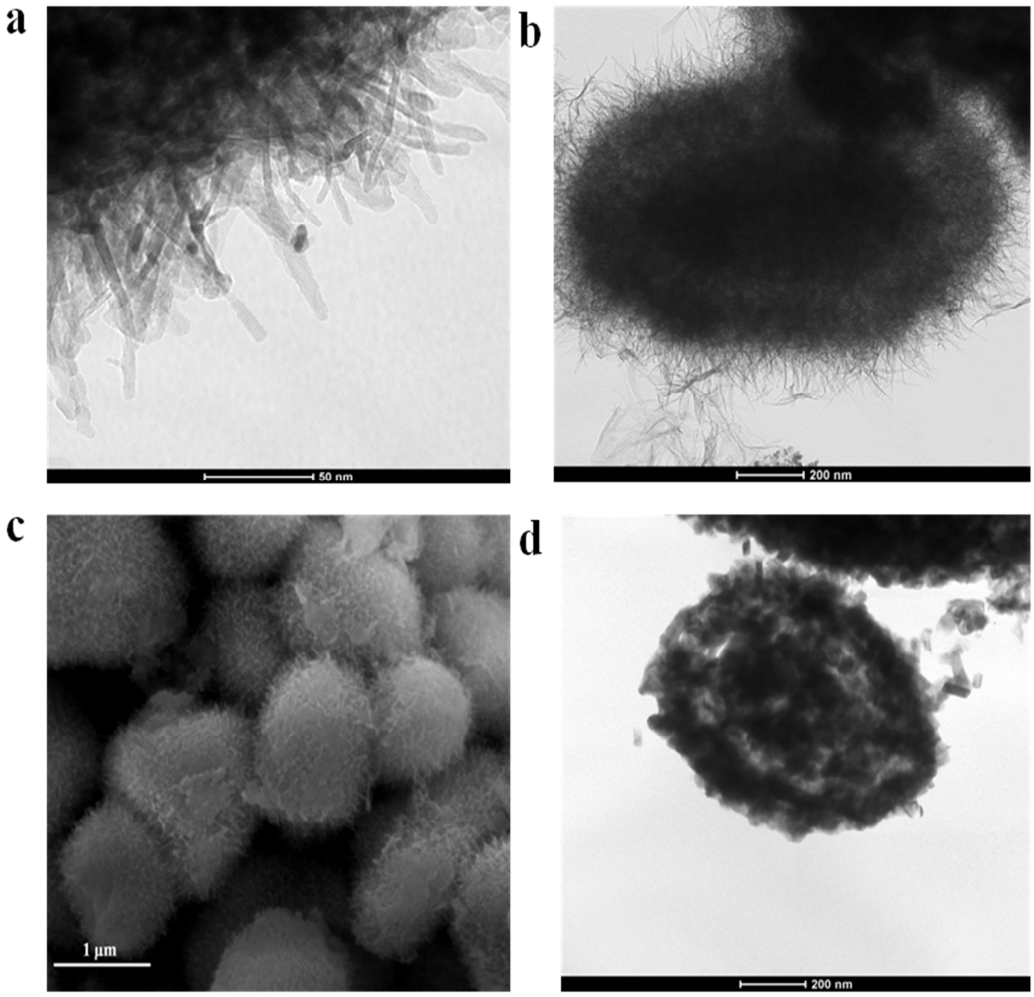


Fig. 3 TEM images of (a) $Ti(OH)_4$ nanorods, (b) $Fe@Pt/Ti(OH)_4$, (d) calcined $Fe@Pt/Ti(OH)_4$ at 700 °C. And SEM image of (c) $Fe@Pt/Ti(OH)_4$.

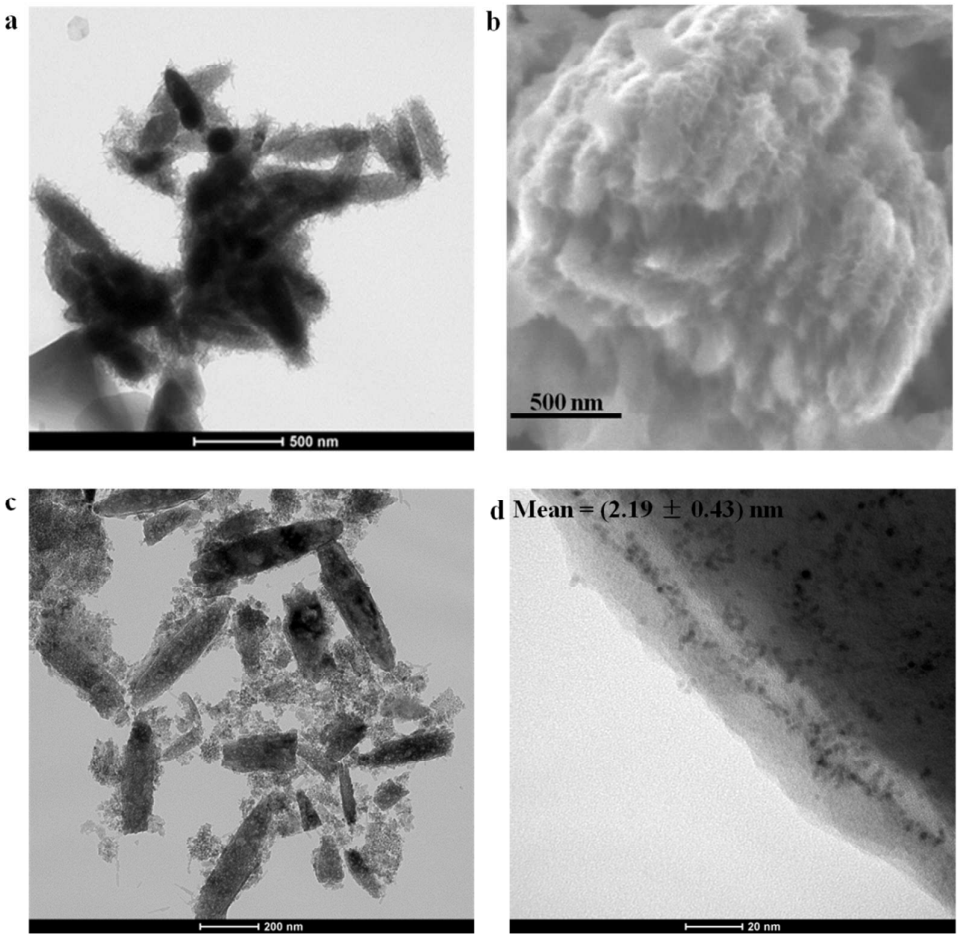


Fig. 4 TEM images of (a) α-$Fe_2O_3$@Pt/$Ti(OH)_4$, (c) calcined α-$Fe_2O_3$@C/Pt/$TiO_2$ at 500 °C without $mSiO_2$ protection, (d) the magnified α-$Fe_2O_3$@C/Pt/$TiO_2$. And SEM image of (b) α-$Fe_2O_3$@Pt/$Ti(OH)_4$.

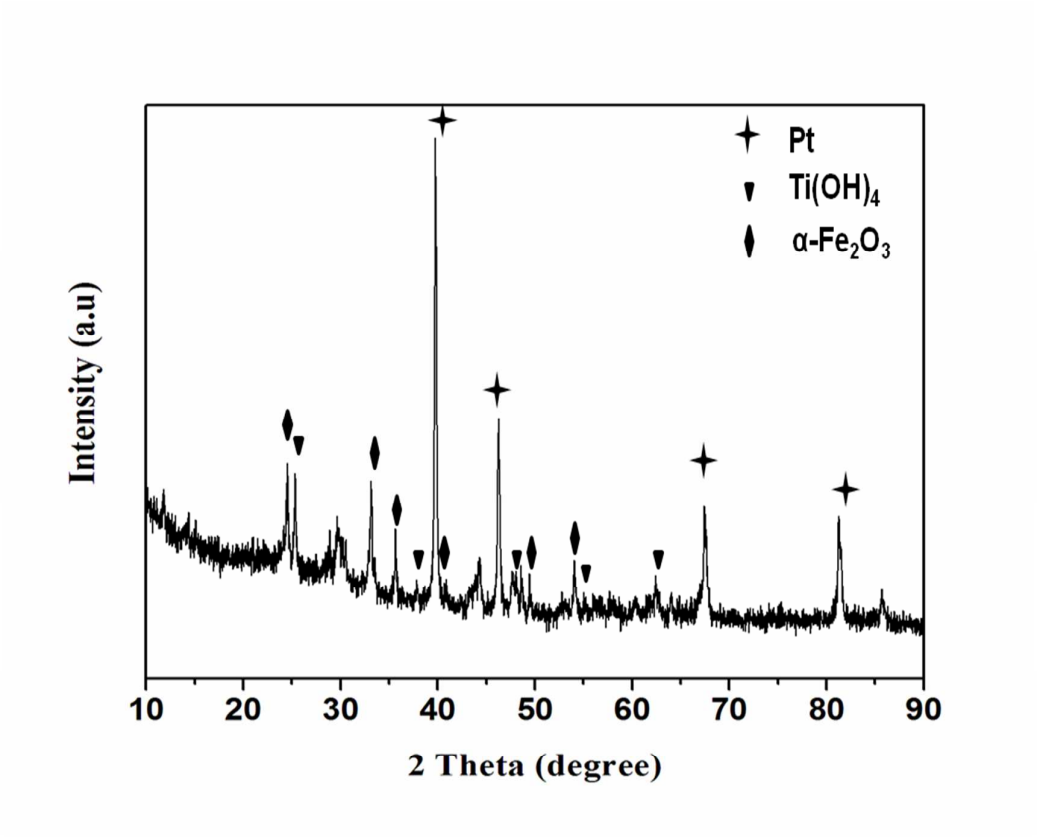


Fig. 5 XRD pattern of cancined α-$Fe_2O_3$@Pt/$Ti(OH)_4$ at 500 °C.

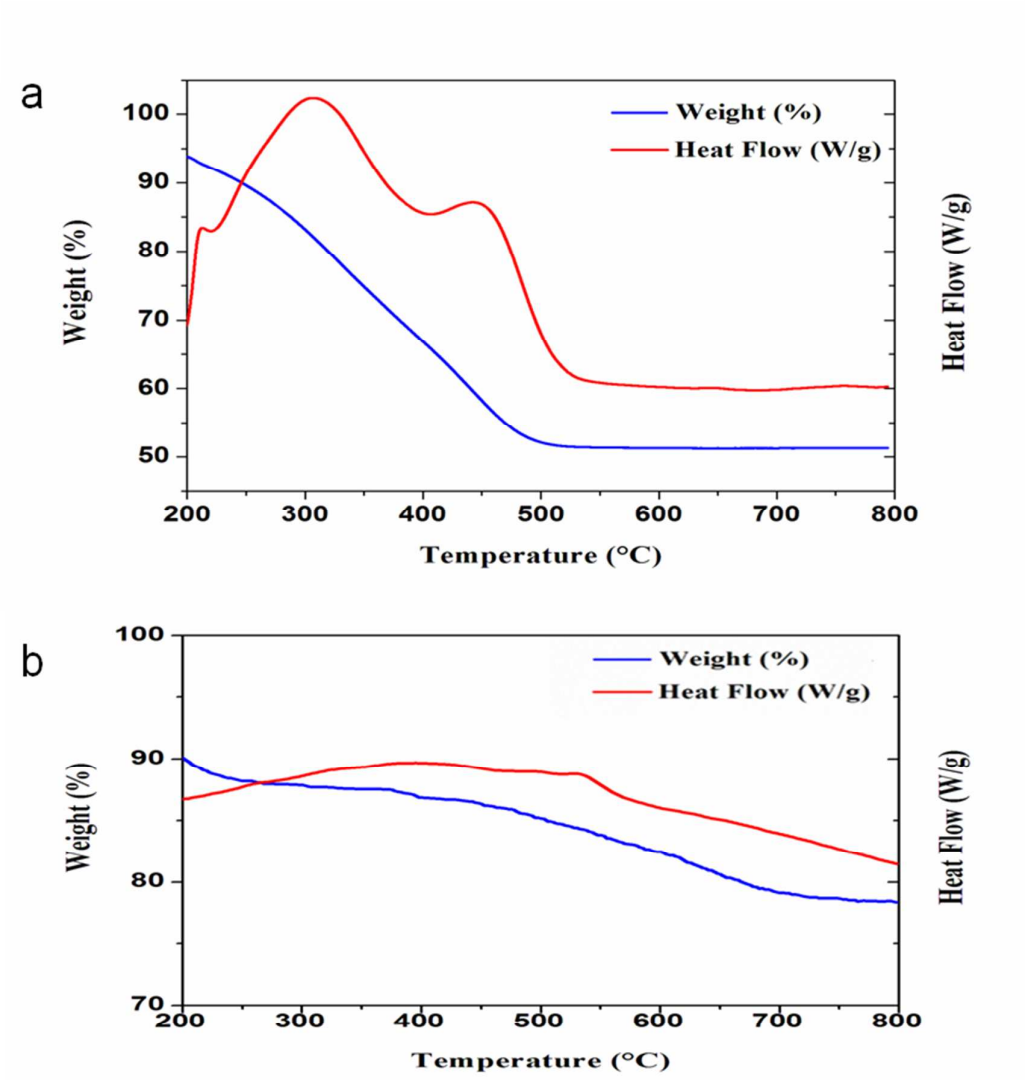


Fig. 6 TGA curves for (a) α-$Fe_2O_3$@C/Pt/$TiO_2$/m$SiO_2$ and (b) α-$Fe_2O_3$@Pt/$Ti(OH)_4$.

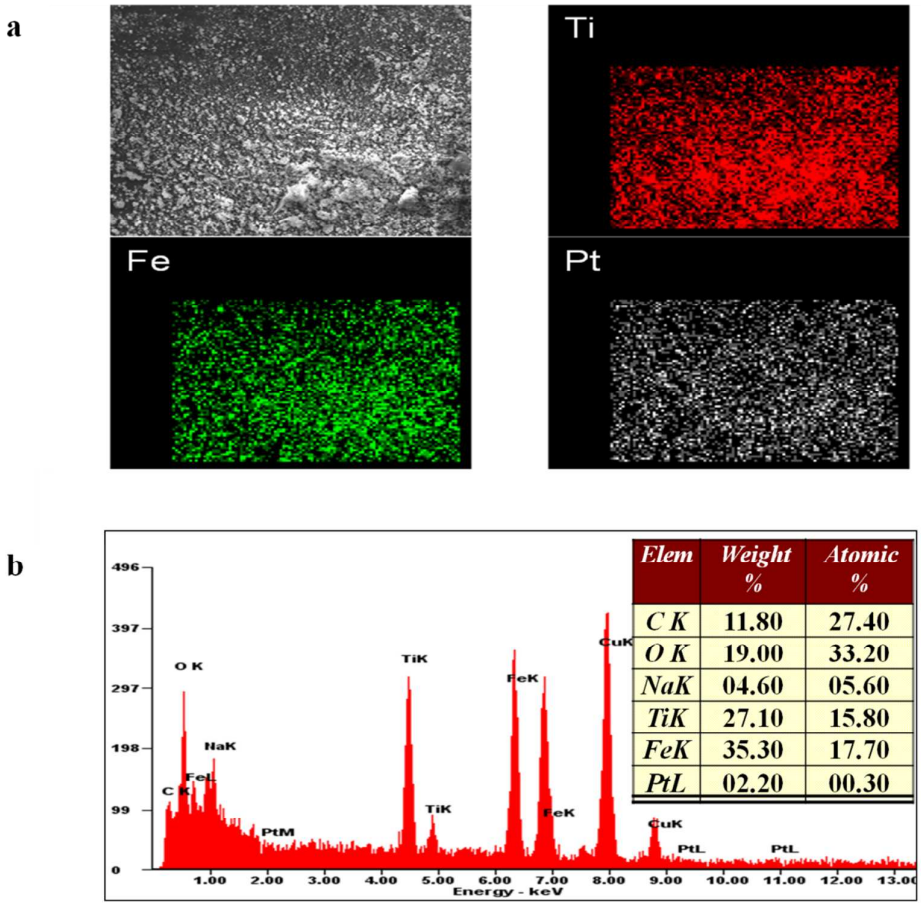


Fig. 7 (a) EDX mapping analysis and (b) EDX analysis of Fe@Pt/Ti(OH)$_4$.

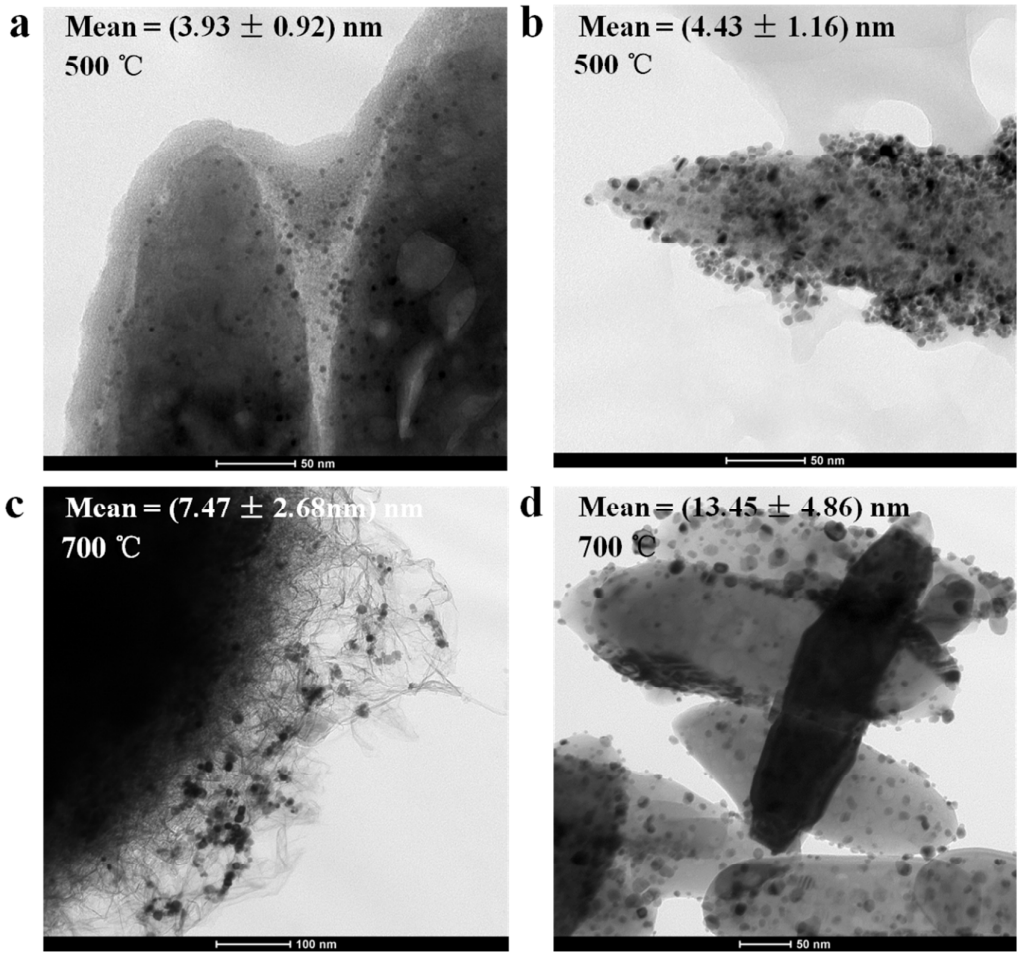


Fig. 8 TEM images of (a) calcined α-$Fe_2O_3$@C/Pt/$TiO_2$/m$SiO_2$ at 500 °C, (b) calcined TN at 500 °C (TN500), (c) calcined α-$Fe_2O_3$@C/Pt/$TiO_2$/m$SiO_2$ at 700 °C and then treated with concentrated NaOH solution, (d) calcined TN at 700 °C (TN700). All the samples were calcined in air for 4 h.

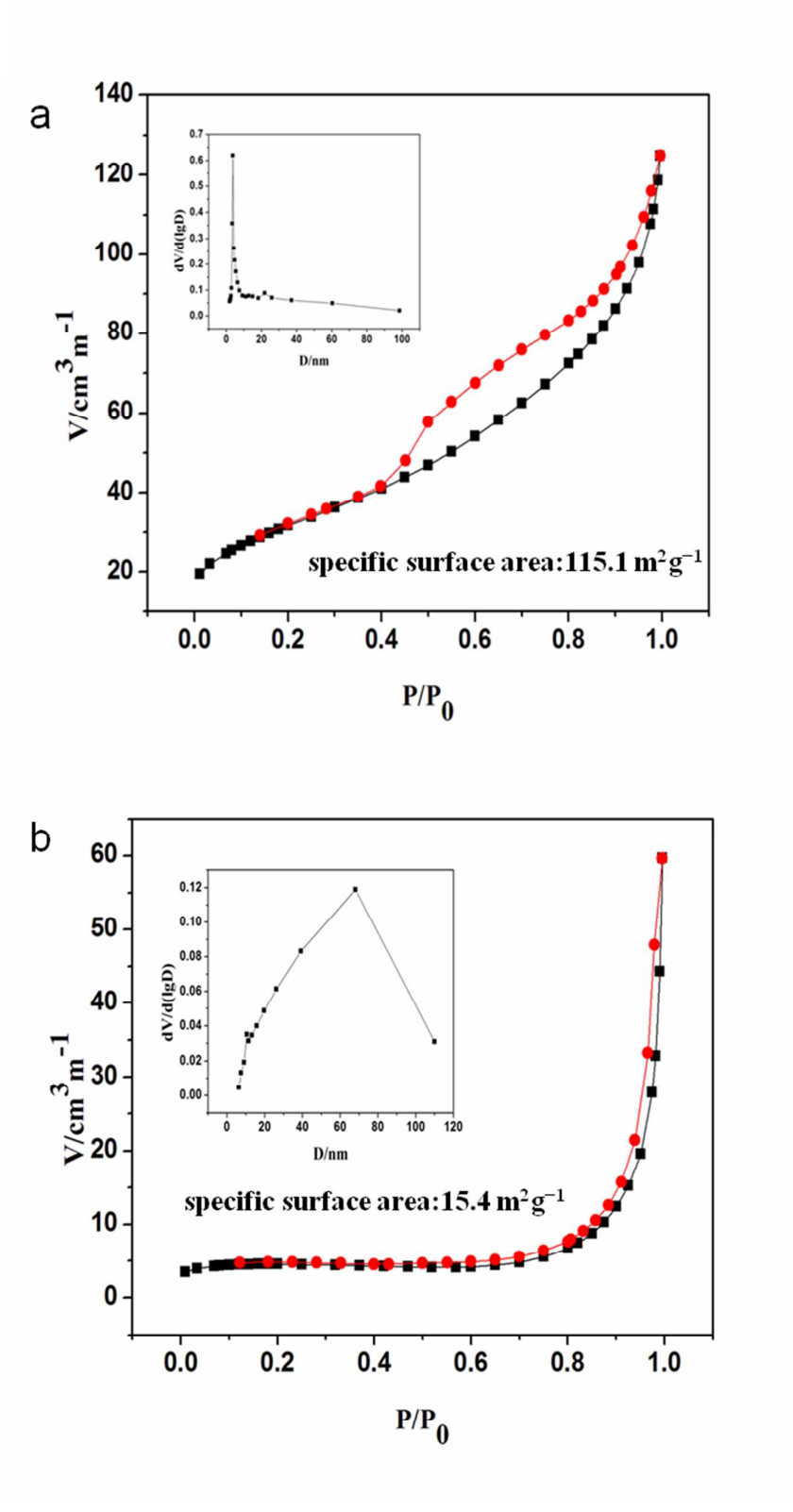


Fig. 9 Nitrogen adsorption–desorption isotherms of (a) α-$Fe_2O_3$@Pt/$Ti(OH)_4$ and (b) traditional "naked" α-$Fe_2O_3$@$TiO_2$/Pt sample. The inset is the pore size distribution.

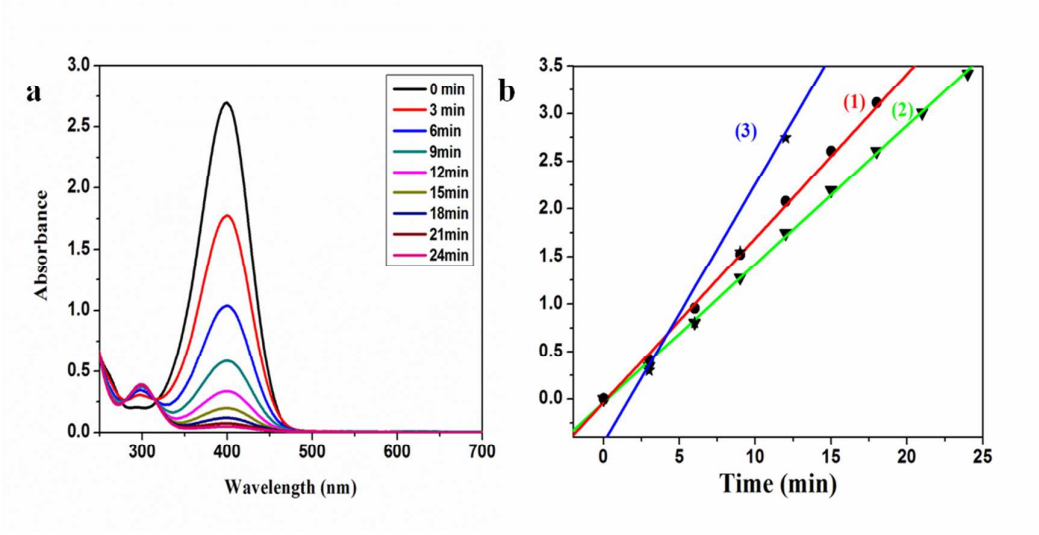


Fig. 10 (a) Variation in UV-vis spectra at 3 min intervals for the 4-NP reduction in the presence of Fe@Pt/Ti(OH)$_4$. (b) ln($C_t$/$C_0$) versus the reaction time over different samples: (1) Fe@Pt/Ti(OH)$_4$ (HMN), (2) calcined HMN at 500 ℃ in air (HMN500), (3) calcined HMN at 700°C in air (HMN700).

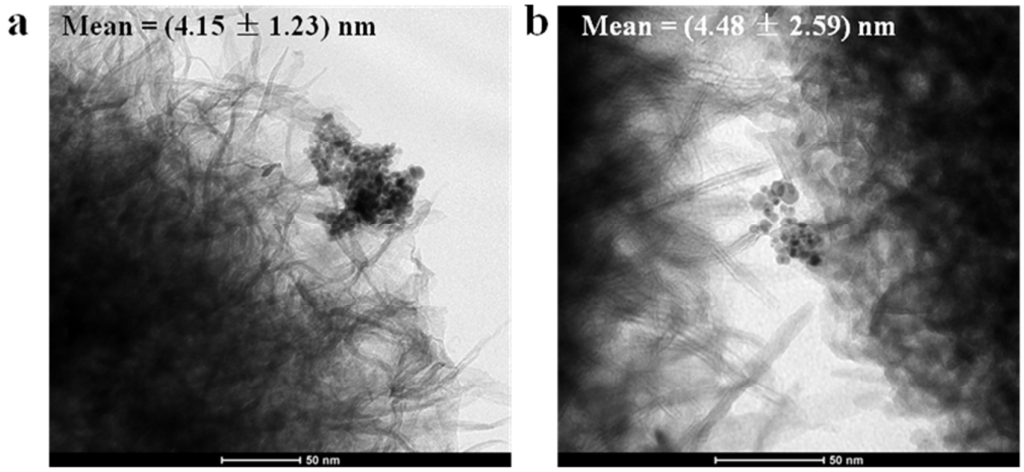


Fig. 11 TEM images of (a) Fe@Pt/$Ti(OH)_4$ (HMN), (b) calcined HMN at 500 °C in air for 4h (HMN500)

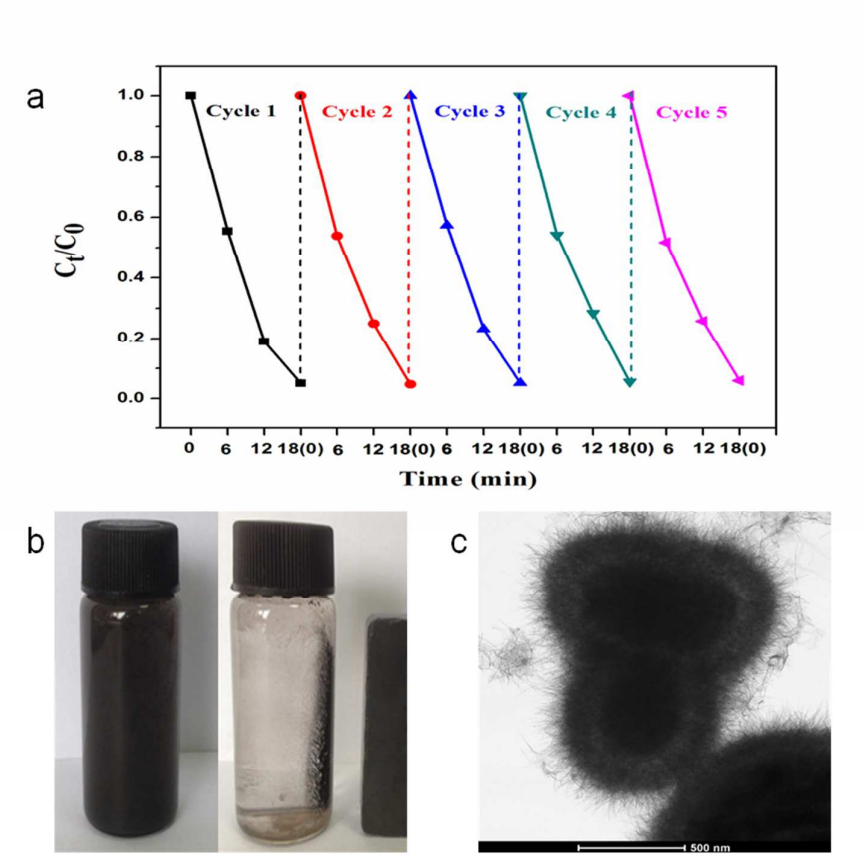


Fig. 12 (a) $C_t/C_0$ as a function of the reaction time in five successive reduction using HMN catalyst, (b) the images of magnetic separation, (c) TEM image of the final HMN catalyst.